Interdecadal Thermocline Variability in the North Pacific for 1958–97: A GCM Simulation*

SHANG-PING XIE

International Pacific Research Center/SOEST, University of Hawaii, Honolulu, Hawaii

TATSUGA KUNITANI+ AND ATSUSHI KUBOKAWA

Graduate School of Environmental Earth Science, Hokkaido University, Sapporo, Japan

MASAMI NONAKA

International Pacific Research Center/SOEST, University of Hawaii, Honolulu, Hawaii

SHIGEKI HOSODA

Graduate School of Environmental Earth Science, Hokkaido University, Sapporo, Japan

(Manuscript received 16 July 1999, in final form 28 December 1999)

ABSTRACT

An ocean general circulation model is forced with the NCEP reanalysis wind stress for 1958–97 to understand mechanisms of ocean subsurface variability. With relatively high horizontal ($1^\circ \times 1^\circ$) and vertical (41 levels) resolutions, the model produces mode waters on a range of density surfaces in the western, central, and eastern North Pacific, in qualitative agreement with observations.

These mode waters appear as a thermostad or a region of weak stratification in the upper thermocline as they flow southward from their formation regions in the Kuroshio and its extension. In the model, subsurface temperature variability in the central subtropical gyre reaches a maximum within the thermostad, in contrast to what might be expected from the linear baroclinic Rossby wave theory. This variance maximum is associated with the longitudinal shift in the path of mode waters. In particular, deepened mixed layer and accelerated eastward currents in the Kuroshio Extension by wind changes in the mid-1970s act cooperatively to move the central mode waters toward the east, causing large subsurface temperature anomalies.

Besides the local maximum in the central North Pacific subtropical gyre, two additional maxima of the subsurface anomaly are identified in the northwestern and southern parts of the gyre, respectively. Among these subsurface anomaly centers, the one in the northwestern North Pacific has a strong effect on the model sea surface temperature, suggesting that the Kuroshio and its extension are a key region to decadal/interdecadal ocean–atmosphere interaction. Finally, possible effects of atmospheric thermal forcing are discussed.

1. Introduction

Recent observational studies reveal that the North Pacific ocean–atmosphere system displays substantial variability from interannual to interdecadal timescales (Tanimoto et al. 1993; Trenberth and Hurrel 1994; Graham 1994), with important consequences to the nutrient distribution and fishery resources in the North Pacific (Polovina et al. 1995; Mantua et al. 1997) and to the climate over North America (e.g., Minobe 1997). Such decadal or longer variability in sea surface temperature (SST) appears in coupled ocean–atmosphere models, with spatial structures similar to the observations (Latif and Barnett 1994; Yukimoto et al. 1996; Robertson 1996; Knutson and Manabe 1998). With its large heat content, the ocean is widely believed to provide the memory and set the slow timescales for such decadal and longer variability. Mechanisms involving oceanic Rossby waves (Jin 1997; Neelin and Weng 1999), gyre circulation (Latif and Barnett 1994), and a subtropical–tropical water path way (Gu and Philander 1997; Kleeman et al. 1999) have been proposed,

* International Pacific Research Center Contribution Number 53 and School of Ocean and Earth Science and Technology Contribution Number 5254.

+ Deceased.

Corresponding author address: Dr. Shang-Ping Xie, International Pacific Research Center/SOEST, University of Hawaii, 1000 Pope Road, Honolulu, HI 96822-2285.
E-mail: xie@soest.hawaii.edu

but their validity remains to be tested with further numerical experiments.

A major recent climatic event, often referred to as the climate regime shift, occurred in the mid-1970s over the North Pacific (Nitta and Yamada 1989). Around 1975–76, the Aleutian low and subtropical westerly winds strengthened, causing a SST decrease of up to 1°C over the central North Pacific. Using historic oceanographic data, Deser et al. (1996) and Yasuda and Hanawa (1997) examined subsurface changes associated with this mid-1970s event. Their decadal difference fields before and after 1975 display a subsurface cooling centered on the 25.5 isopycnal or the 15°C isothermal in the central North Pacific. A natural extension of this earlier work is to analyze the full cycle of the subsurface variability whose phase is likely to vary substantially over the North Pacific due to waves and other delay processes. The current subsurface ocean dataset does not allow such an analysis because of the insufficient number of observations. The situation is worsened as these few observations are likely to be contaminated by synoptic oceanic eddies that generally have much larger amplitudes than decadal variability.

Ocean general circulation models (OGCMs) thus become indispensable in understanding the variability below the ocean surface. Recent GCM simulations with observed surface momentum and heat fluxes as forcing seem successful in reproducing many observed features of subsurface variability in the North Pacific (Miller et al. 1994, 1998). Much of our understanding of the oceanic response to surface wind changes is based on the ventilated thermocline theory (Luyten et al. 1983), where atmospheric forcing can be divided into dynamic (Ekman pumping) and thermodynamic (SST) components. When a winter SST anomaly is produced, it is subducted into and advected on the main thermocline (e.g., Liu 1999). In OGCMs, Nonaka et al. (2000) and Schneider et al. (1999a,b) show that this subduction–advection mechanism is indeed consistent with the observed southwestward spreading of subsurface cooling associated with the mid-1970s climate regime shift. In thermocline models, surface cooling can be treated as a southward shift of the outcropping line (e.g., Huang and Pedlosky 1999). Ekman pumping, on the other hand, is known to generate first baroclinic mode Rossby waves (Anderson and Gill 1975), a mechanism Miller et al. (1998) confirm in a realistic OGCM simulation.

The present study investigates the dynamic response of an OGCM to changing surface wind stress. Our strategy is to force a widely used, standard OGCM (Geophysical Fluid Dynamics Laboratory Modular Ocean Model) with a dynamically consistent wind product and identify the dominant mechanisms of variability. For wind stress, we use output from the NCEP reanalysis (Kalnay et al. 1996), which is arguably better than shipboard wind measurements themselves, which are often sparse and contaminated by synoptic-scale weather. The reanalysis takes into account concurrent surface pressure measurements and therefore provides better representation of large-scale wind field in off-equatorial regions where geostrophy prevails. As a further deviation from previous simulations of the North Pacific variability, we use variable wind stresses but restore SST and sea surface salinity (SSS) to their climatology for the following reasons. First, surface heat flux product contains larger errors than the wind stress and additional surface thermal forcing is often introduced by restoring the model SST toward observed interannual SST field. Interannual variability in surface freshwater flux is even more uncertain and previous simulations ignore it all together. Second, the absence of anomalous atmospheric buoyancy forcing[1] allows us to focus on the dynamic response of the ocean to Ekman pumping. An important question is whether additional mechanisms other than the gravest baroclinic mode of Rossby waves might dominate certain parts of the ocean. Third, because SST variability in the model can be exclusively attributed to ocean dynamics, this wind-stress-only simulation offers a unique opportunity for identifying the key regions where subsurface processes can impact on SST.

The main thermocline in the ocean is often modeled as a layer where density stratification reaches a local maximum in the vertical direction. The vertical motion of this maximum stratification layer is known to be a major mechanism for ocean subsurface temperature variations as most clearly seen in an El Niño event (e.g., Xie 1995). In the subtropical gyre, however, the stratification within the thermocline is not uniform, but varies substantially both in the vertical and horizontal directions. In particular, the Brunt–Väisälä frequency reaches a local minimum within the so-called subtropical mode water, which appears as a peculiar thick layer in a longitude–depth section of isopycnals (McCartney 1982). Recent theoretical (Kubokawa and Xie 1999, manuscript submitted to *J. Phys. Oceanogr.*) and idealized GCM studies (Inui et al. 1999) indicate that this weakly stratified mode water might change its longitude in response to variable Ekman pumping. The present study confirms that such mode water variability indeed takes place in a GCM run under realistic settings, suggesting that it can potentially be a major mechanism for subsurface temperature variability in a large portion of the subtropical gyre.

The rest of the paper is organized as follows. Section 2 introduces the model and wind forcing. Section 3 gives a brief overview of model variability, of which the mode water is a major source. Section 4 then describes isopycnal distribution of potential vorticity and discusses

[1] Surface heat flux is a function of both SST and atmospheric, thermal forcing that is just the reference temperature the model SST is restored toward here. The model SST will vary with time due to anomalous Ekman flow and gyre circulation. Thus, surface heat flux also changes with SST, but the anomalous atmospheric thermal forcing has been set to zero.

mode water's formation mechanisms. Section 5 links the mode water variability to wind changes and section 6 is the summary. Readers who are only interested in temporal variability may skip section 4 and proceed to section 5.

2. Model and wind forcing

We use the GFDL Modular Ocean Model (MOM1.1: Pacanowski et al. 1991), an OGCM widely used for ocean circulation and climate research. The model covers the portion of the Pacific Ocean from 50°S to 60°N, and has realistic coast line and bottom topography with a maximum depth of 5000 m. The model solves the primitive equations in spherical coordinates under the Boussinesq, rigid lid, and hydrostatic approximations. The horizontal and vertical eddy viscosities are constant at 10^8 and 10 $cm^2\ s^{-1}$, respectively. Tracers (temperature and salinity) are mixed both along (Cox 1987) and across isopycnal surfaces with diffusivities of 2×10^7 and 0.3 $cm^2\ s^{-1}$, respectively. The model employs the nonslip condition and requires the fluxes of mass, temperature, and salinity to vanish at all the side boundaries and bottom. Within 5° of the poleward boundaries, temperature and salinity are restored to the monthly climatology (Levitus 1982). At the sea surface, an observed monthly mean wind stress is applied, and SST and SSS are restored to their monthly climatologies with a time constant of 70 days for a water column 50 m deep. The horizontal resolution of the model is 1° in both longitudinal and latitudinal directions, at the high end of noneddy resolving models. There are 41 vertical levels with a resolution of 10 to 15 m in the top 300 m. The high vertical and horizontal resolutions reduce numerical diffusion and improve the simulation of conservative properties such as salinity (Nonaka and Takeuchi 1999, manuscript submitted to *J. Phys. Oceanogr.*) and potential vorticity. The conservation of the latter forms the foundation of the ventilated thermocline theory. (Luyten et al. 1983).

We use the monthly mean surface wind stress data derived from the NCEP reanalysis (Kalnay et al. 1996) for a 40-yr period from January 1958 to December 1997. The reanalysis maintains the same model assimilation system for the 40-yr period and utilizes all the available in situ and satellite measurements. Particularly, the assimilation of sea surface pressure (SLP) observations has a major impact on surface wind stress product on large scales as SLP measurements suffer less from sampling errors than wind measurements.

Forced by the monthly mean climatological wind stress derived from the above 40-yr dataset, the OGCM is spun up for 30 years from a resting state with the Levitus (1982) temperature and salinity stratification. To reduce the initial shock due to the wind change, we run the model for another 10 years during which the wind stress forcing is gradually changed from the climatology to the 1958 field. Then the model is forced with the real-time NCEP wind for 40 years from January 1958 to December 1997. The following analysis uses winter (Jan–Mar) mean data from the last 40-yr simulation. We define the model climatology as the average for the last 30 years (1968–97).

3. Subsurface variability

We first show in Fig. 1a the root mean square (rms) of temperature anomalies at 200-m depth to facilitate comparison with similar previous studies. There are three centers of action: in the Tropics at 15°N, the Kuroshio Extension around 40°N, and central subtropical gyre around 34°N, 160°W, in the order of variance. The model time series of an area-averaged 400-m temperature anomaly in the Kuroshio Extension (Fig. 2a) compares favorably with Deser et al.'s (1996) Fig. 13. The time–depth section indicates that the temperature variations are in phase in the vertical direction with a maximum at 200 m, the depth of the main thermocline. As in many similar type models, the model Kuroshio separates from the Japanese coast at a too northern latitude with a too broad extension compared with observations (e.g., Qiu 2000). Despite these deficiencies in the climatological simulation of these strong nonlinear currents, the model's success in reproducing decadal variability suggests that linear baroclinic Rossby waves are the cause of the variability, in support of Miller et al. (1998). Whereas surface heat flux is almost certainly a contributing force in the real Pacific (Yasuda and Hanawa 1997; Tanimoto et al. 1997; Miller et al. 1998), the SST decrease in the 1980s in the Kuroshio Extension is caused by ocean dynamics in the model since the SST is restored toward the climatology. Analogous to the eastern equatorial Pacific, the Kuroshio Extension region may thus be a key region to North Pacific ocean–atmosphere interaction, where remotely forced oceanic waves can alter SST and hence trigger changes in atmospheric circulation.

The tropical rms maximum along 14°N (Fig. 1a) seems to have an observational counterpart (Zhang and Levitus 1997). Here we compare the model longitude–time section of 200-m temperature anomalies at 14°N (Fig. 1c) with observations compiled by White (1995). Three-year running averages are applied to the observations to reduce the sampling errors. Generally the model compares quite favorably with observations except before 1965 when the model produces a strong warming not seen in observations. The model amplitudes are slightly large compared to observations, presumably due to either wind errors or smoothing in gridding observed data. The model subsurface anomalies display a tendency for westward phase propagation, indicative of Rossby waves, which is less clear in gridded observational data. In particular, a cold Rossby wave first appears in the model at 140°W in 1976 and then travels westward. The wave-induced cooling arrives in the western Pacific two to three years later, consistent

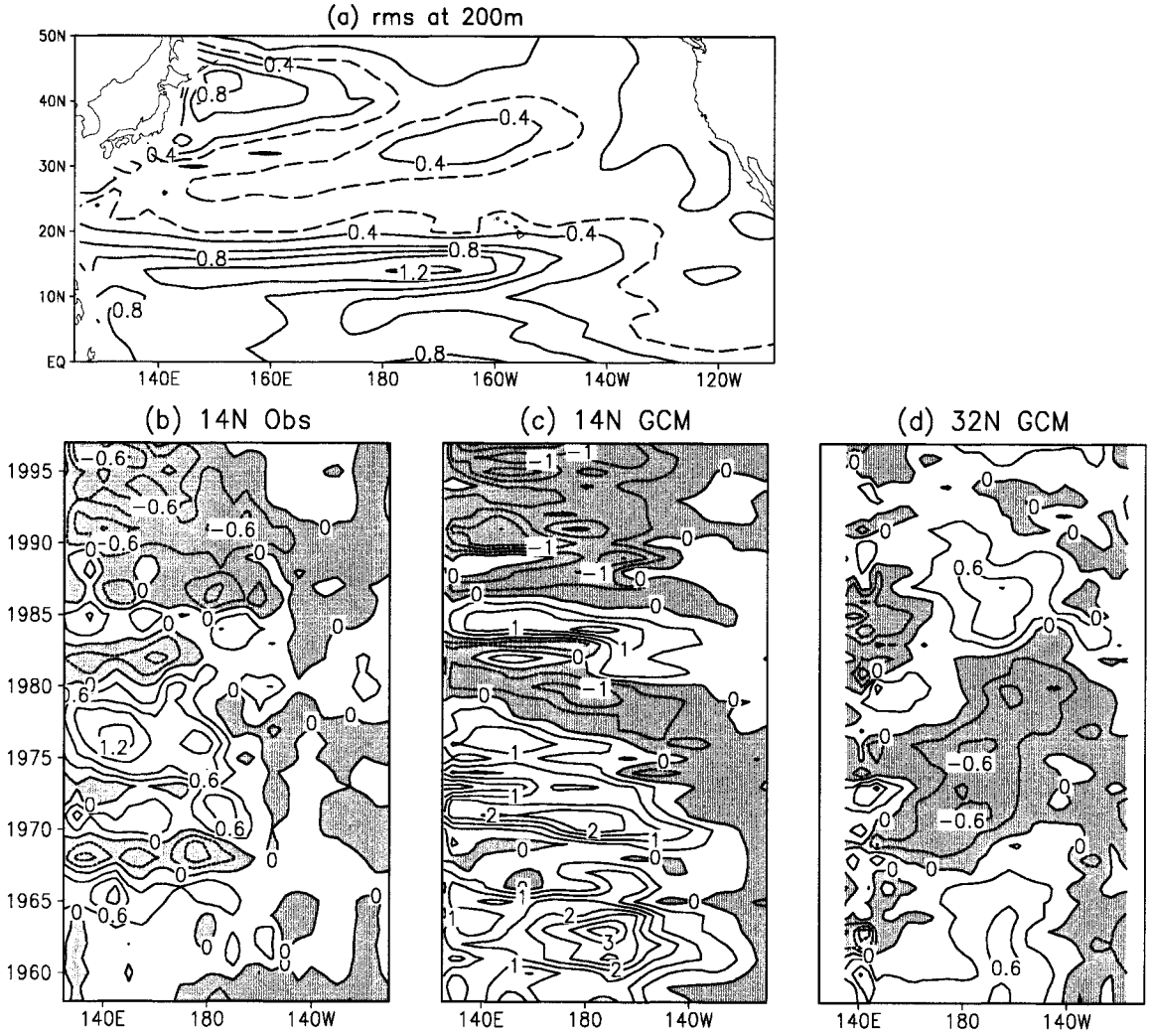

FIG. 1. (a) Standard deviation (°C) of temperature variability at 200 m. Longitude–time sections of 200 m temperature anomalies (negative shaded) at 14°N in (b) observations and (c) the GCM. (d) As in (c) except at 32°N.

with Japanese observations along the 137°E line (Shuto 1996). A comparison with the 137°E section data indicates that the model succeeds in capturing nearly all the interannual wave events south of the Kuroshio since the observation started in 1967 (F. Bingham 1999, personal communication).

Most previous studies focus on variability within vertical levels of fixed depth. But Figs. 2 and 3a indicate that the subsurface temperature variability in both the Kuroshio Extension and Tropics is associated with vertical motion of the main thermocline. Thus it seems more appropriate to examine the model variability on isopycnal surfaces instead of at fixed depths. Figure 4 depicts the depth rms on the $\sigma_t = 25.5$ surface. The tropical and Kuroshio Extension variance maxima remain, but the maximum in the central subtropics becomes much more prominent, dominating the depth variance field. The rms variance in the central subtropics reaches 70 m, four times that at the other two local maxima.

In the southern subtropical gyre, the depth of maximum temperature variability closely follows that of maximum vertical stratification (Fig. 3a), indicative of the first baroclinic mode. In the north-central subtropical gyre, by contrast, the temperature variability reaches its maximum in a region of minimum stratification in the permanent thermocline (Fig. 3b). The weak stratification in the upper part of the permanent thermocline is sometimes called thermostad and corresponds to the so-called mode water defined here as a zonal minimum in isopycnal potential vorticity (PV),

$$Q = \frac{f}{\rho}\frac{\partial \rho}{\partial z},$$

where f is the Coriolis parameter, ρ is the water density,

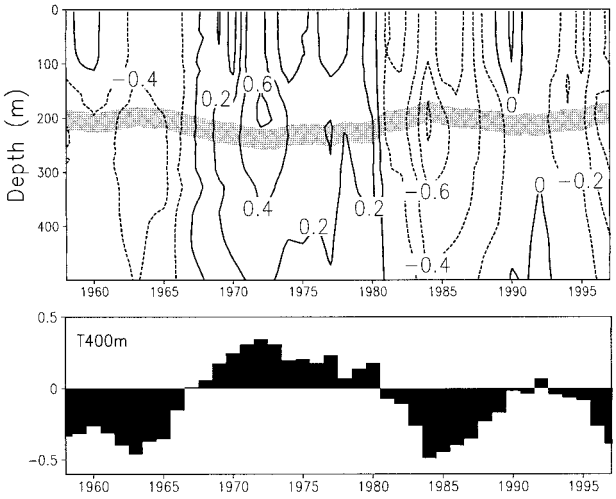

FIG. 2. Upper panel: Time–depth section of temperature anomalies (°C) averaged in the Kuroshio Extension region (34°–42°N, 140°E–180°), with the 25.6–25.8 density layer shaded. Lower: Same area-average temperature anomaly at 400 m as a function of time.

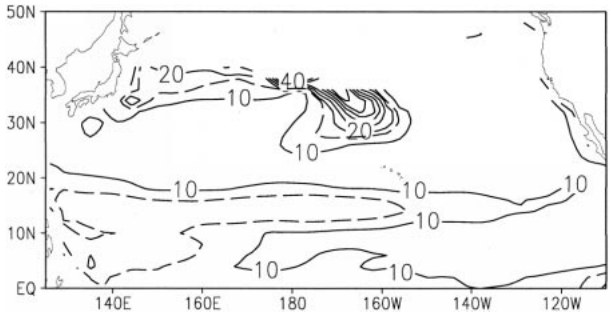

FIG. 4. Standard deviation (m) of depth variability on the 25.5 density surface. The 15-m isoline is dashed.

and z the vertical coordinate. Yasuda and Hanawa (1997) have shown a similar climatological PV minimum that slants downward and eastward in longitude–depth sections, but their observed climatological minimum is much less prominent. The model/forcing errors may be at fault, but the extensive time–space averaging in constructing the climatology may act to smooth out the PV minimum that has relatively small zonal scales.

The peculiar association of the low PV water with subsurface temperature variability in Fig. 3 will be the

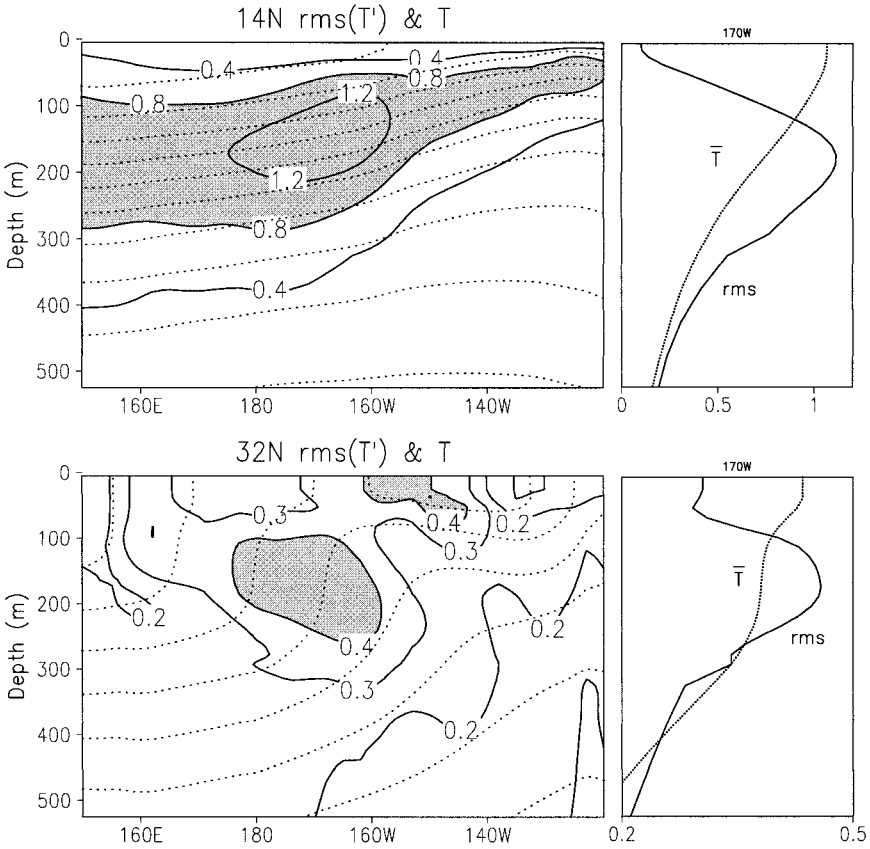

FIG. 3. Standard deviation (°C) of temperature variability at 14°N (upper) and 32°N (lower panel). In the left panels, mean isothermals are plotted in dotted lines. The right panels show profiles of mean temperature (dotted) and standard deviation (solid line) at 170°W.

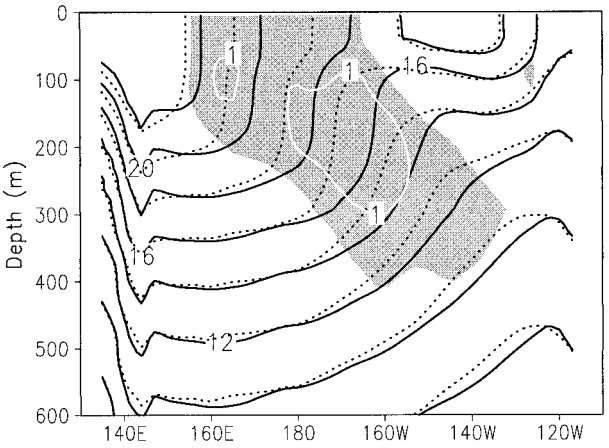

FIG. 5. Longitude–depth sections of temperature at 32°N in 1987 (solid) and 1977 (dotted) and their difference (shade > 0.5°C).

focus of the rest of the paper. The longitude–time section of 200-m temperature anomalies at 32°N (Fig. 1d) indicates that variability in the low PV region centered on 170°W favors decadal to interdecadal timescales and experiences two major phase-flipping events in the mid-1960s and early 1980s, respectively. To see what causes these subsurface temperature changes, we superimpose the total temperature fields at two extreme opposing phases in 1987 and 1977, along with their differences (shade > 0.5°C, Fig. 5). Relative to the 1977 field, the core of the low PV (mode) water shifts substantially eastward, giving rise to a warming of up to 1.0°C. The temperature differences are aligned with the low PV region, further in support of the key role by the mode water.

The subduction and advection of SST anomalies are not the cause of the warming associated with mode waters colder than 16°C because the SST in their formation region decreases around the mid-1970s (see section 5 and Fig. 14b). Instead, some dynamic mechanism unique to the mode water is responsible. It should be noted that SST anomalies are much larger in the real Pacific than in this model, forcing subsurface temperature anomalies that take a route overlapping this low-PV region (Nonaka et al. 2000). So the observed variability in the mode water region is likely caused by both Ekman pumping and SST/atmospheric thermal forcings. Nevertheless, we feel it useful to isolate and study this dynamic mechanism involving the mode water because it is an interesting problem by itself, one that might reveal some new ocean dynamics. Furthermore it can serve as a stepping stone to better understand more realistic simulations incorporating atmospheric thermal forcing. Because of the possible effect of additional SST forcing, the present study will focus more on the dynamics of subsurface variability than on the realism of the wind forcing-only simulation. We plan to conduct a simulation with combined wind stress and SST forcing, whose results will be compared with observations and reported elsewhere.

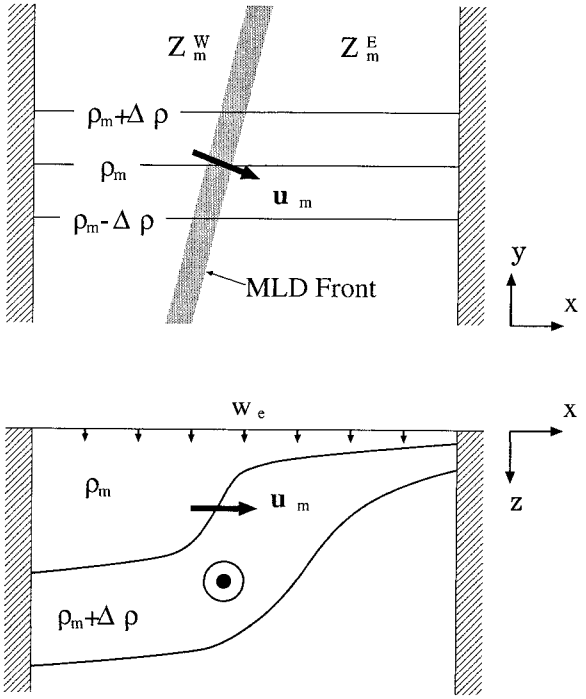

FIG. 6. Schematics of mode water formation due to a rapid zonal variation in the MLD. Upper: A plane view of surface density (contour) distribution. The deep mixed layer region to the northwest is separated from the shallow region by a sharp MLD front (shade). Lower: A longitude–vertical view of isopycnals at the latitude where the ρ_m density surface outcrops.

4. Mode water formation

Before going into further details of the temporal variability, we need to know how the low-PV mode water is formed in the model. Following an argument by Kubokawa (1999), we first consider an idealized case where the surface density is zonally uniform and the mixed layer is deep in the west and shallow in the east (Fig. 6). For simplicity, further assume that the mixed layer depth (MLD) distribution is piecewise uniform with $z_m^W > z_m^E$ with a narrow transition zone called the *MLD front* separating the deep and shallow mixed layer regions. Here z_m^W (z_m^E) denotes the MLD in the west (east). Kubokawa shows that the potential thickness—the inverse of potential vorticity—subducted from the mixed layer can be expressed as

$$q \equiv \frac{1}{f}\frac{\partial z}{\partial \rho} = \frac{1}{f}\left[\left(\frac{\partial z_m}{\partial \rho_m}\right)_{\mathbf{u}_m} + \frac{w_m}{\mathbf{u}_m \cdot \nabla \rho_m}\right], \qquad (1)$$

where the subscript m denotes variables at the bottom of the mixed layer, $\mathbf{u}$ and w are horizontal and vertical velocities, respectively [see also Williams (1991) Eq. (4)]. The subscript in $\mathbf{u}_m$ denotes that the derivative, $\partial z_m/\partial \rho_m$, is taken in the direction of the current at the bottom of the mixed layer. The second term in the parenthesis does not change very much in the zonal direction if the wind stress curl is zonally uniform.

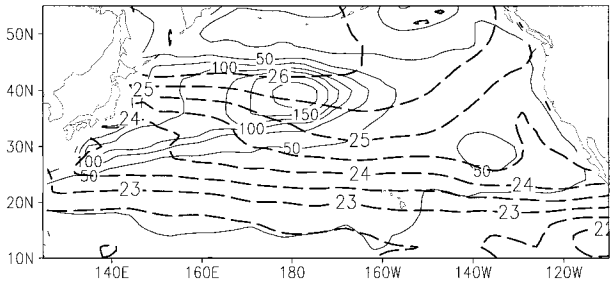

FIG. 7. Winter surface density (thick dashed) and MLD (thin contours) distributions in the model. The bottom of the mixed layer is defined as the depth where σ_t first exceeds its surface value by 0.05 kg m^{-3}.

The first term vanishes in most regions except within the MLD front where it records large values. Therefore the mode water of zonal maximum potential thickness (or minimum PV) on a given isopycnal forms where the outcrop line intersects the MLD front. From their intersection, the low-PV mode enters the main thermocline, advected southward by the Sverdrup gyre flow and conserving its PV in the inviscid limit. The crosspoint between an outcrop line and MLD front will be called the *entrance point* hereafter.

Here one point needs clarification. The northward deepening of the mixed layer does not give rise to a marked zonal maximum in potential thickness as is evident in Eq. (1). It is the rapid zonal—or more generally along-outcropping line—variation in the MLD that leads to a pronounced PV minimum localized in the interior subtropical gyre as depicted schematically in the lower panel of Fig. 6.

Figure 7 shows the winter surface density and MLD distributions averaged for the last 30 years of the model run. The bottom of the mixed layer is defined each winter as the depth where σ_t first exceeds its surface value by 0.05 kg m^{-3}. Overall, the surface density field resembles observations as a consequence of restoring boundary conditions. But near the western boundary and in the Kuroshio extension region, the model density is appreciably lower than the observed because of the heat transport by the Kuroshio. The model MLD field is roughly similar to the observed one [e.g., Fig. 1 of Huang and Qiu (1994)] with a deep mixed layer in the northwestern subtropical gyre over the Kuroshio and its extension. As in observations, the MLD maximum is located roughly at 40°N and extends eastward up to 170°W. The deep and shallow mixed layer regions are separated by a narrow zone—the MLD front. The southern MLD front tilts northeastward and intersects the outcrop lines of densities between σ_t = 23.5 and 26 in the model. This tilt of the MLD front in Huang and Qiu's observations is less clear and stays more or less along 30°N.

Figure 8 depicts potential vorticity (solid) on four isopycnals along with their outcrop lines (dashed). The 100-m MLD isoline (dotted) is also plotted to mark the position of the MLD front. The low PV water enters

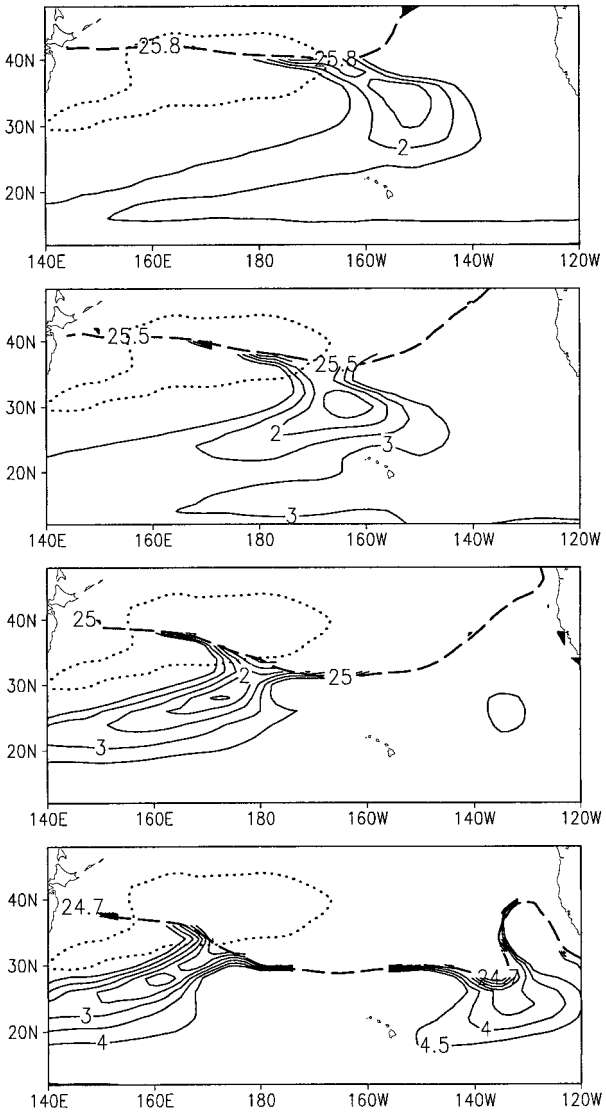

FIG. 8. Climatological mean potential vorticity (10^{-10} m^{-1} s^{-1}) on the σ_t = 25.8, 25.5, 25.0, and 24.7 surfaces. Only small values are plotted for clarity. The outcrop line for each isopycnal is plotted in dashed line whereas the 100-m MLD contour is dotted to mark the MLD front.

the main thermocline at the crosspoint of the outcrop line and MLD front much as envisioned by Kubokawa (1999). Similar low PV water formation has been noted by Kubokawa and Inui (1999) in an idealized GCM experiment. Following their entrance point shift, heavier mode waters form successively to the northeastward of the lighter ones. After entering the main thermocline, a mode water is advected southward by the gyre flow and leaves a distinct low PV tongue on the isopycnal. Despite the isopycnal diffusion scheme and high spatial resolutions that substantially reduce the numerical diffusion, the PV minimum in the low PV tongue diffuses away on its path southward, particularly on heavier isopycnal surfaces. Right after being subducted into the main thermocline, the PV anomaly of the mode water

is so large that it creates a large zonal density gradient (Figs. 3b and 5), which is diffused by the weak background horizontal diffusion that has to be incorporated to maintain the model computational stability.

Observed PV maps [e.g., Fig. 4 of Talley (1988)] show a similar tendency for the formation region of the mode water to shift northeastward as its density increases. The PV minimum on these observed maps is much less pronounced than in the model. Observations identify two major mode waters in the North Pacific, the subtropical mode water (STMW: Suga and Hanawa 1990; Bingham 1992) on $\sigma_t = 25.4$ and central mode water (CMW: Nakamura 1996; Suga et al. 1997) on $\sigma_t = 26.2$. Here the term "mode water" is interchangeable with a localized PV minimum, a much broader terminology than that in descriptive oceanography. Because of the warm bias in the mixed layer temperature in the Kuroshio and its extension, the model mode waters form on lighter density surfaces than in observations. This warm bias in the northwestern North Pacific is a defect common to all GCMs that restore SST back to the observed climatology.

Very recently Hautala and Roemmich (1998) identified another mode water in the northeast Pacific in a density range of $\sigma_t = 24$–25.4. This eastern subtropical mode water (ESTMW) is well captured in the model (Fig. 8). On the $\sigma_t = 24.7$ isopycnal, there are two local PV minima. The weaker one in the east corresponds to Hautala and Roemmich's ESTMW. The PV map based on the model temperature output gives a similar eastern PV minimum (not shown), lending support to Hautala and Roemmich's temperature-based analysis. The realistic simulation of ESTMW is largely owing to the weak currents in its formation region, so the model density does not deviate far from the imposed climatology.

As pointed out by Hautala and Roemmich (1998), the formation of this ESTMW is puzzling because winter cooling apparently is not the cause as it is for the other western mode waters. Here we apply Eq. (1) and infer the initial values of the ESTMW potential thickness. The first term in the parenthesis is unimportant here as the MLD does not change much and w_m is also more or less spatially uniform except near the coast. A maximum in potential thickness forms because the horizontal gradient of surface density field is small as indicated by the increased opening between the 24.5 and 25 surface density isolines near 30°N, 140°W (Fig. 7).

The initial PV upon subduction can be determined by recasting Eq. (1):

$$Q = -\frac{f}{\rho}\frac{\mathbf{u}_m \cdot \nabla \rho_m}{S} \approx \frac{f\tilde{u}_m}{SL}\frac{\delta\rho}{\rho}, \qquad (2)$$

where S is subduction rate (Williams 1991), $\tilde{u}_m$ and L are horizontal velocity and distance measured along the surface density gradient. There are two ways to form low PV water: by increasing the subduction rate (S) and by widening the distance between two outcropping lines (L). In our model, the enhanced subduction rate due to lateral induction is responsible for the western mode waters, whereas the eastern mode water forms because of the diffluent outcropping lines. The former has been discussed extensively in the literature (Marshall and Nurser 1991; Williams 1991; Huang and Qiu 1994; among others). Even with a uniform subduction rate S, low PV waters can still form because the total volume of subducted water—SL, the denominator of the rhs of (2)—between two isopycnals can be enhanced by increasing the distance between their outcropping lines. Lateral induction may also play a role in the ESTMW formation because there is a weak maximum in both the MLD and subduction rate (Qiu and Huang 1995).

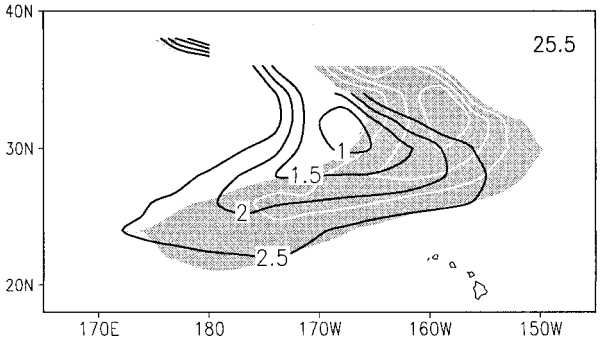

FIG. 9. Potential vorticity distributions on the $\sigma_t = 25.5$ surface in 1987 (shade) and 1977 (black contours).

5. Mode water path changes

Now we return to the temporal subsurface variability and attempt to link it to changes in wind forcing. In the following, the isopycnal surfaces are computed at each time of the analysis. Figure 9 contrasts isopycnal PV distributions at two extreme phases of the temporal variability, showing a large eastward shift of the low PV tongue in the 1980s. In particular, the low PV tongue takes a more eastward path before turning southwestward in the 1980s than in the 1970s. Associated with this zonal shift in the low PV tongue, the upper thermocline sinks as much as 100 m, giving rise to large subsurface temperature anomalies (Fig. 5).

To see the full cycle of the temporal evolution, we plot in Fig. 10 the longitudes of isopycnal PV minima at several latitudes as functions of time. During the 40-yr model run, the mode water core experiences large shifts in the east–west direction with a range of as much as 10° longitude. At 36°N, two major events occur to the low PV water: a westward shift in late 1960s and an eastward one in early 1980s. To the south at 32°N, similar events are found and there is a tendency for these events to take place on deeper isopycnals at successively later time. The time delay between the $\sigma_t = 25.2$ and 26 surfaces for the 1980s event is about three years. The longitudinal shift in the low PV minima is still discernible further south at 28°N but is contaminated by higher frequency interannual variability.

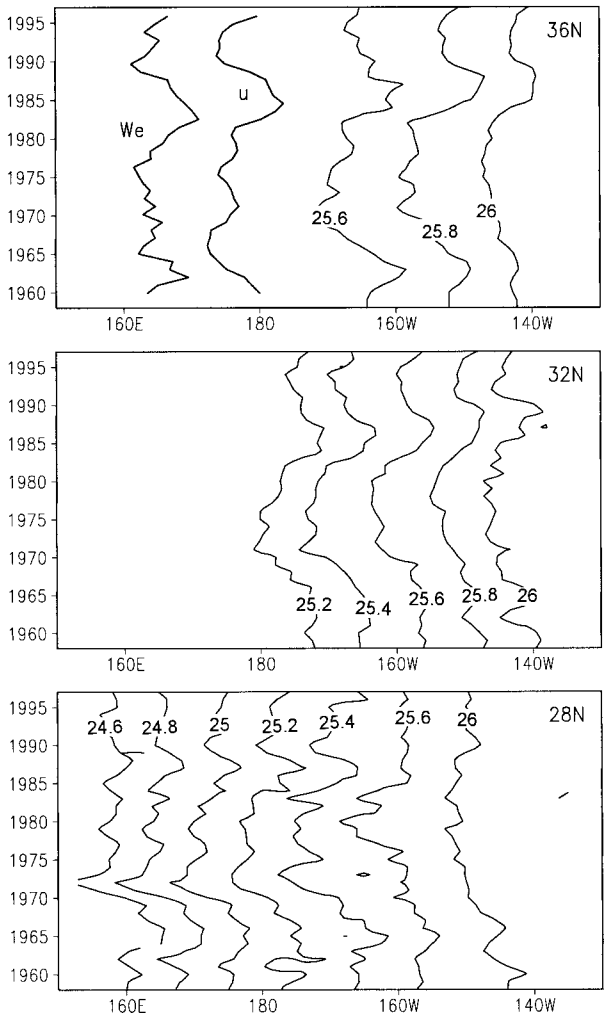

FIG. 10. Longitude of zonal potential vorticity minimum as a function of time on isopycnals at 36°N, 32°N, and 28°N. Area-average Ekman pumping (We: 34°–42°N, 180°–140°W) and $\sigma_t = 26$ zonal current (u: 34°–38°N, 170°W–140°W) velocities are plotted in the upper panel as functions of time.

It is well known that the westerly winds over the North Pacific strengthened around the mid-1970s (Nitta and Yamada 1989), as is clear from the latitude–time section of 180°–140°W average wind stress anomalies (Fig. 11a). There is a brief period in the late 1980s when the westerlies relax. Overall, the wind stress anomalies are out of phase between 32° and 50°N, displaying a dipolar structure indicative of the latitudinal shift in the westerly jet. The Ekman pumping velocity (upward positive),

$$w_e = \text{curl}(\boldsymbol{\tau}/f)/\rho = [\text{curl}(\boldsymbol{\tau}) + \tau_x\beta/f]/(f\rho), \qquad (3)$$

forces the thermocline directly and is a quantity more relevant to thermocline variability than either wind stress or its curl. Here $\boldsymbol{\tau}$ is the wind stress, τ_x its zonal component, ρ water density, and β is the latitudinal derivative of the Coriolis parameter. The Ekman pumping velocity anomalies appear more prominently near the nodal point of the wind stress dipole, reaching their maxima at 40°N. Another major w_e anomaly center is in the Tropics between 10° and 20°N, which forces large thermocline variability at 15°N (Fig. 1). The w_e anomalies are generally small between 20° and 30°N as the bracketed terms in (3) cancel each other. Figure 12 depicts the difference fields before and after the wind regime shift. The zonal wind stress anomalies are more or less zonally uniform south of 35°N—the axis of the anomalous westerlies—whereas to the north a cyclonic anomalous circulation exists. To first order, the forcing for thermocline variability associated with the mid-1970s wind regime shift is dominated by anomalous Ekman upwelling between 32° and 55°N.

It follows from Sverdrup theory that the ocean responds to this Ekman pumping forcing by generating anomalous eastward geostrophic flow in the northern subtropical gyre, which indeed happens in the model (Fig. 13). The acceleration of the eastward flow peaks around 1980, about five years after the wind shift. The phase of zonal current anomalies is rather uniform in the vertical within the main thermocline (not shown), indicating that they are associated with the first baroclinic mode. On the $\sigma_t = 25.8$ surface, we see well-organized anomalous eastward flows as part of a cyclonic circulation between 30° and 40°N. To the south, the anomalous flow field features a weaker anticyclonic circulation. All this is consistent with the linear Sverdrup theory. We superimpose the low PV tongues for 1979 and 1987, three years after the current velocity extremes, respectively. The accelerated eastward flows in early 1980s advect the low PV water farther eastward compared to that in the mid-1970s. For a mean southward Sverdrup flow of 1 cm s^{-1}, it takes the low PV water three years to reach 32°N after entering the main thermocline at 40°N. Anomalous zonal currents between 32° and 40°N are about 1 cm s^{-1}, which can move the path of the low PV water eastward by 10° longitude when it reaches 32°N. This is in rough agreement with Fig. 13. Farther to the south, the anomalous currents change their direction to the west, reducing the zonal excursion of the mode water (see also Fig. 9).

Changes in the formation region of the mode water can also cause its path to change. Figure 14a depicts the longitude–time section of the 5-yr running mean MLD at 38°N. The MLD variability is modest in the deep ML region but large at the surrounding MLD front. The MLD front begins a rapid eastward advancement in the mid-1970s, resulting in a local depth increase of up to 100 m from 1974 to 1976 in the unfiltered data (not shown).[2] A

[2] The rapid climate regime shift around mid-1970s are the dominant change in the North Pacific, but there are other wind variabilities with different time–space structures that can affect the ocean particularly near the surface. Both this richness in forcing specturm and the fact that the MLD is affected not only by the local forcing at the surface but by geostrophic dynamics beneath contribute to the complex behavior of the MLD. In the deep mixed-layer region west of 175°W in Fig. 14a, for example, the MLD peaks in 1975, in the middle of the major wind regime shift.

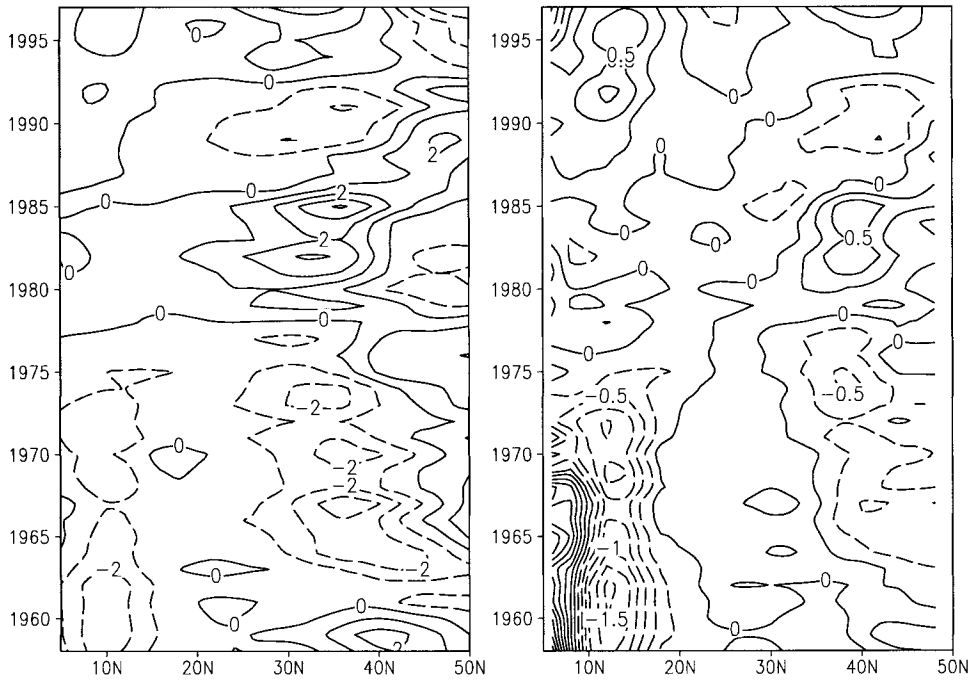

FIG. 11. Latitude–time sections of zonal wind stress (left in 10^{-2} N m^{-2}) and Ekman pumping velocity (right in 10^{-6} m s^{-1}) anomalies averaged between 180° and 140°W. A 5-yr running mean filter is applied.

similar deepening of the mixed layer following the mid-1970s wind regime shift is observed in the central North Pacific (Polovina et al. 1995; Deser et al. 1996) and simulated in an ocean GCM forced by both observed wind stress and total heat flux (Miller et al. 1994). Figure 14b shows the 5-yr average MLD front (solid) and surface density (dashed) centered on 1970 and 1987, the extreme phases of the MLD variability. The deep mixed layer region shifts eastward and expands southward in the 1980s compared to that in 1970. Whereas the low-PV-water entrance point—the crosspoint of the MLD front and outcropping line—does not change much for isopycnal surfaces of large densities, it shifts eastward in 1987 as much as 7° longitude for the σ_t = 24.5–25.5 density range. On these isopycnals, changes in the formation region are presumably important for the eastward shift of the low PV water to the south.

To demonstrate the advective mechanism for changes in the mode water path, we release passive particles on 1 March each year at the mode water entrance point and

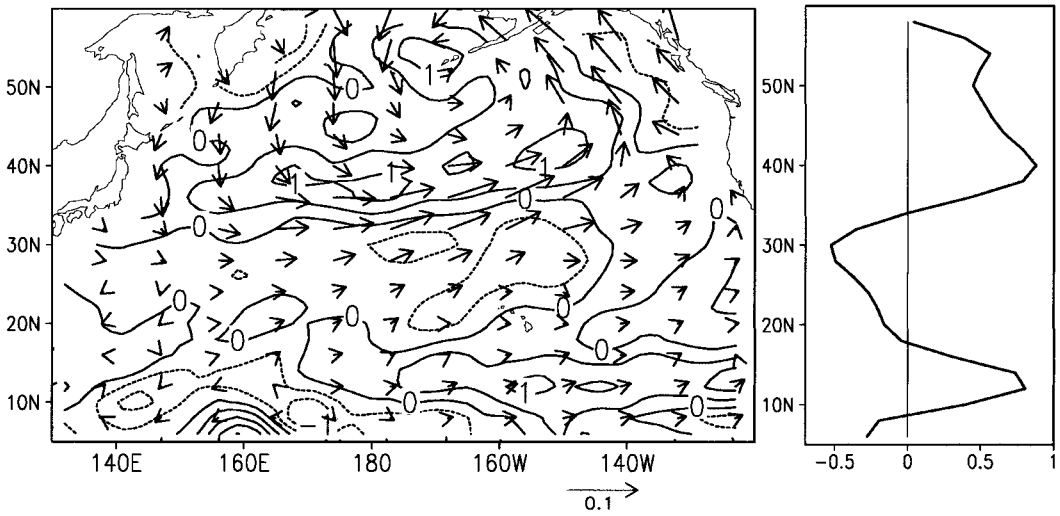

FIG. 12. Wind stress (vectors in N m^{-2}) and Ekman pumping velocity (contours in 10^{-6} m s^{-1}) differences between 1977–86 and 1965–74. The right panel shows the 180°–140°W average Ekman pumping velocity difference.

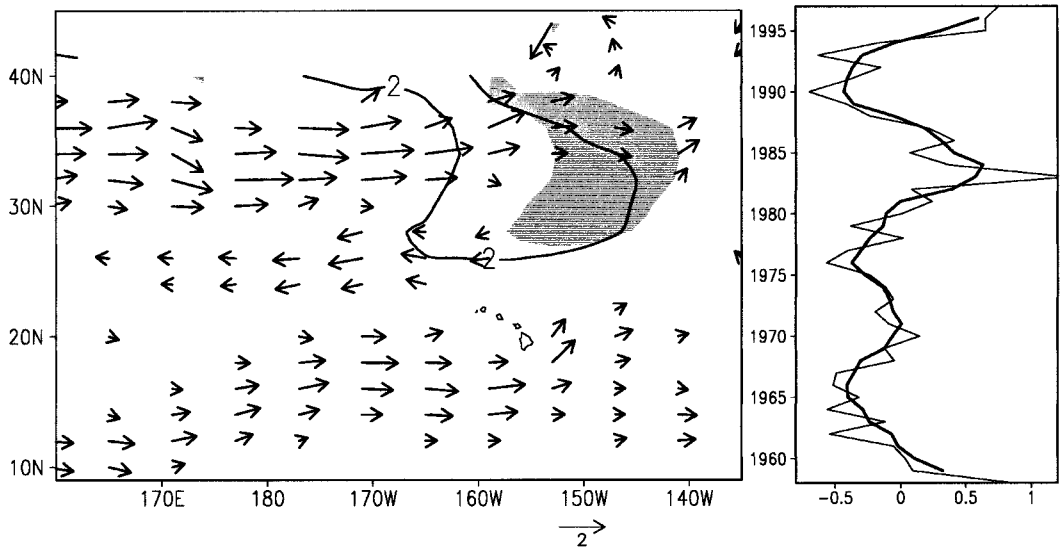

FIG. 13. Left: Current velocity difference (vectors in m s^{-1}) between 1983–85 and 1975–77 on the $\sigma_t = 25.8$ isopycnal surface, along with the low PV tongues in 1987 (shade $< 2 \times 10^{-10}$ m^{-1} s^{-1}) and 1979 (contour). Right: Zonal current velocity anomaly averaged in the middle North Pacific (32°–38°N, 170°W–140°W; thin) on the same isopycnal and its 3-yr running mean (thick line) as a function of time.

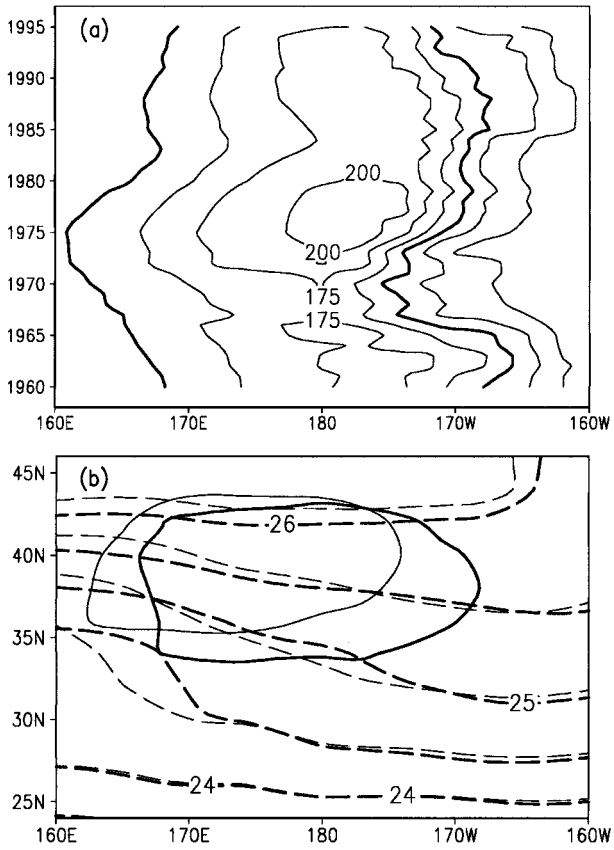

FIG. 14. (a) Longitude–time section of 5-yr running mean MLD (m) at 38°N. (b) The MLD (solid) and surface density (dashed) distributions in 1984–88 (thick) and 1968–72 (thin contours). The 125-m MLD contour denotes the MLD front.

advect them with the model flow field. Figure 15a shows the time and longitude at which these particles arrive at 32°N. The trajectories of these passive particles capture quite well the movement of the low-PV core on each isopycnal. We have filled the marks for those particles released between 1975 and 1985 to highlight the major eastward excursion. Thus it becomes clear that both the passive particle and low-PV core on the 25.8 surface lag 2–3 years behind their counterparts on the 25.4 surface in reaching their easternmost positions. This time lag arises because a heavier mode water has to travel a longer distance to 32°N than a lighter one. Figure 15c displays the trajectories of particles released between 1975 and 1985 on the 25.8 surface. There is a clear separation in the longitude that the early and late particles reach at 32°N. On this isopycnal, changes in the velocity field are the dominant cause. Whereas the 1979 and 1985 particles enter the main thermocline at about the same longitude, they end up 8° apart at 32°N down to the south. The 1985 particle also takes one year longer to reach 32°N than the 1979 one, consistent with the reduced southward Sverdrup flow in Fig. 13.

In an idealized GCM experiment, Inui et al. (1999) report that, in response to wind stress changes confined to the northern subtropical gyre, the low PV water changes its path even at latitudes well south of the forcing region. Whereas Inui et al. attribute the shift in mode water formation region as the cause, Kubokawa and Xie (1999, manuscript submitted to *J. Phys. Oceanogr.*) show that a similar shift in the path of mode water can be achieved by changes in advection velocity alone without the MLD and surface density variations in an inviscid ventilated thermocline model. In our GCM,

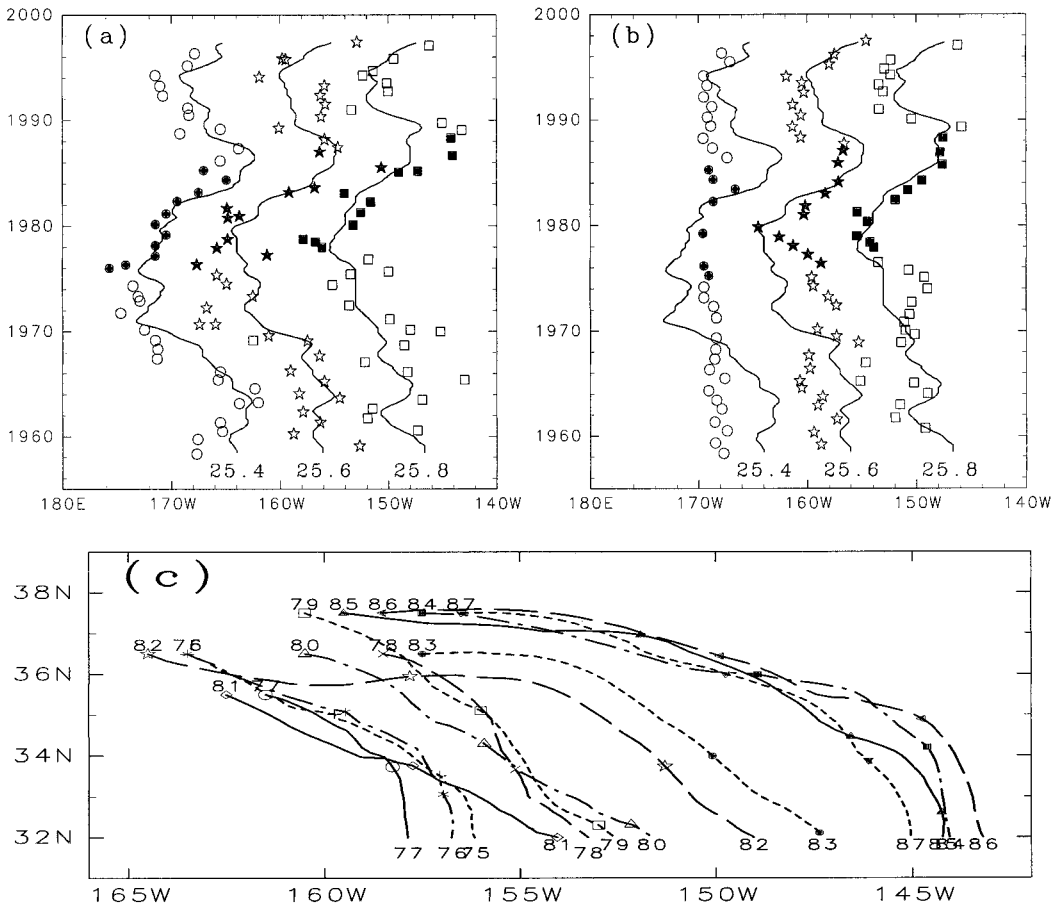

FIG. 15. (a) Longitudes of passive particles (symbols) when they arrive at 32°N, along with the PV minimum lines on the 25.4, 25.6, and 25.8 isopycnals. Particles are released on 1 Mar each year at the entrance point of mode water and advected with the model flow field. Filled symbols are for those released between 1975 and 1985. (b) Same as (a) except that the entrance points are fixed at their climatological mean positions. (c) Trajectories of passive particles on the 25.8 density surface with numerals denoting years of release. A particle takes one year to travel between neighboring symbols on the trajectory.

both formation region and advection velocity vary as winds change, cooperatively shifting the path of the low PV tongue. An additional experiment, where passive particles are released at fixed, climatological-mean entrance points, indicates that changes in advection velocity (entrance point) are the major cause of mode water path excursion on dense (light) isopycnal surfaces (Fig. 15b), a conclusion consistent with the impression one gets from Fig. 14b.

On the vertical section along 32°N, the low PV core not only changes its longitude but its volume and other properties as well. We define the low PV core as the area bounded by $Q = 1.75 \times 10^{-10}$ m^{-1} s^{-1} (shaded in Fig. 16a) and $\sigma_t = 25.4$, an isopycnal always below the bottom of the winter mixed layer at this latitude. The volume of the low PV core increases substantially from 1970 to the early 1980s (Fig. 16b), accompanied by a decrease in the area-averaged PV (not shown). Figure 16c breaks down this total volume into a distribution on density surfaces. The volume of light low PV water does not change much on decadal timescales. Most of the volume variations seen in Fig. 16b are from water denser than 25.5. As a result, volume-weighted mean temperature of the low PV core increases in association with the decrease in total volume after the late 1970s. These volume changes are equivalent to changes in isopycnal PV and are apparently correlated with the changes in low-PV water path. Whereas the increase (decrease) in surface density (SST) in the formation region of denser mode waters (Fig. 14b) does not explain this apparent Lagrangian warming, diabatic processes can affect the subduction rate and initial PV after the subduction by changing the MLD distribution. Ekman pumping and dissipation can also cause changes in mode water Lagrangian properties. Both this Lagrangian warming and the path shift of the mode water contribute to the Eulerian warming in Fig. 5.

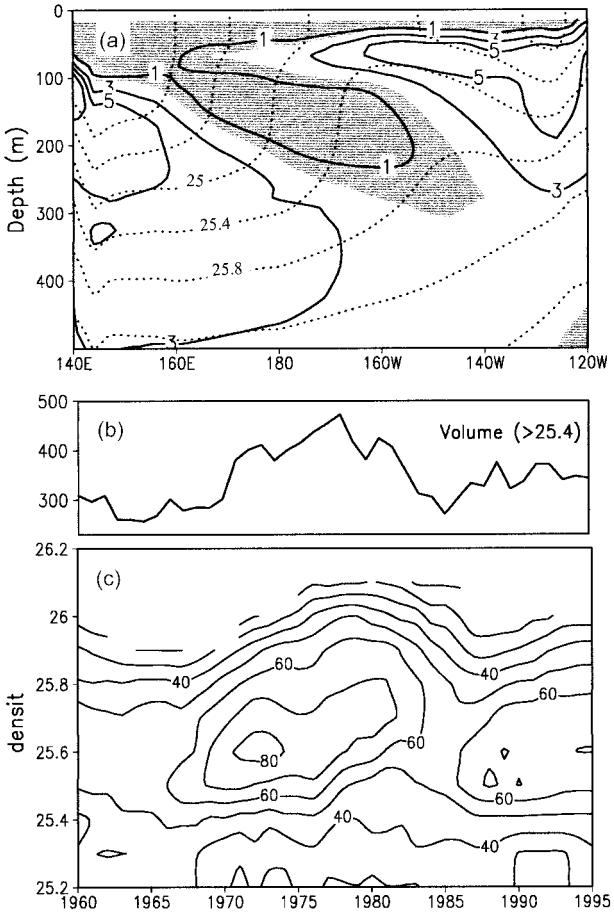

FIG. 16. (a) Potential vorticity (solid; shade $< 1.75 \times 10^{-10}$ m^{-1} s^{-1}) and density (dotted) at 32°N. (b) Total volume (in 10^6 m^2) of the low PV ($<1.75 \times 10^{-10}$ m^{-1} s^{-1}) water denser than 25.4 at 32°N as a function of time. (c) Same as (b) but for volume distribution on density surfaces (in 10^6 m^2 per 0.1 σ_t). Five-year running mean is applied in (c).

6. Discussion

We have forced an OGCM with the newly available NCEP reanalysis wind stress output for 1958–97 in an attempt to simulate the ocean subsurface variability in the North Pacific Ocean. In its climatology, the model is found to produce mode waters or zonally localized potential vorticity minima on isopycnal surfaces of density range σ_t = 24.5–26. Consistent with previous studies, the winter mixed-layer depth distribution is key to the mode water formation. The model mixed layer is deep in the northwestern North Pacific in the Kuroshio and its extension. At the crosspoint of the MLD front and outcropping line, water is inducted from the deep mixed layer into the main thermocline by the southeastward Sverdrup flow, forming a local PV minimum. Because the model MLD front tilts northeastward, the formation region of mode water is found to shift northeastward from south of Japan for light isopycnals to east of the international date line at 40°N. In addition to these western mode waters, the model forms a weaker local PV minimum on the σ_t = 24.5–25 isopycnals in the eastern subtropical gyre, consistent with recent observational findings (Hautala and Roemmich 1998). In contrast to the intense winter cooling mechanism for the western mode waters, the weak horizontal gradient of surface density distribution is the key to formation of the eastern mode water. The large area opening between the outcropping lines allows a large total volume of water to enter the main thermocline between the σ_t = 24.5 and 25 isopycnals, even if the subduction rate per unit area does not display a pronounced maximum.

On a zonal section in the central subtropical gyre, mode waters stack vertically and appear as a weakly stratified region that slants downward, eastward, reflecting the differences in their formation region and advection route. This stacking of mode waters is a distinctive feature of the upper thermocline in the central subtropical gyre, accounting for a large portion of the thermocline water volume. Our results indicate that in the absence of variability in the restoring surface temperature, the change in the longitudinal position of this weakly stratified region is the major mechanism for subsurface temperature/salinity variability in the central subtropical gyre. In the mid-1970s, the surface winds in the North Pacific experience a major regime shift, with the westerly winds shifting its axis southward and intensifying. This wind regime shift deepens the mixed layer in the Kuroshio extension near the international date line, thereby moving the mode water formation region eastward. The associated anomalous upward Ekman pumping further accelerates eastward Sverdrup flow between 30° and 40°N. The shift in the formation region and accelerated eastward currents acts cooperatively to move the path of mode water eastward in 1980s. This eastward shift of the weakly stratified layers depresses the isopycnals to the west, leaving marked temperature anomalies centered on the stacked mode waters (Fig. 5).

Traditionally, the subtropical gyre is divided into three dynamic regimes: pool, ventilated, and shadow zones (Luyten et al. 1983). In response to variable Ekman pumping, variability in the thermocline depth tends to be large around the boundaries of these dynamic zones (Liu 1993). Whereas PV decreases monotonically westward in a ventilated thermocline model without a mixed layer, it has a distinctive minimum within the ventilated zone in the real Pacific Ocean and in our GCM. The ventilated zone may therefore be further divided into regions of eastward and westward PV gradients, separated by the mode water. The notion that the mode water acts as the third dynamic boundary is supported by our model result that thermocline variability indeed reaches a maximum along the PV minimum. Despite its dynamic importance, the realistic representation of mode waters remains a challenge for ocean modeling and requires a realistic simulation of both surface density and mixed-layer depth distributions.

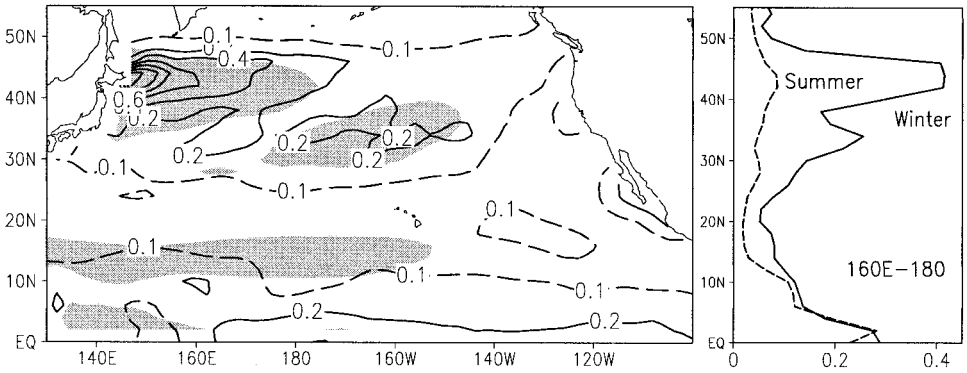

FIG. 17. Standard deviation of SST (contours) and 200-m temperature [shade > 0.3°C (0.6°C) north (south) of 20°N] variability in the model for the boreal winter season. The right panel shows the 160°E–180° zonal averages for winter (solid) and summer (Jun–Aug; dashed).

To focus on the effects of wind stress change on subsurface variability, we choose to restore the model SST and SSS to their observed climatology. The present model output is thus inadequate for a quantitative examination of SST variability, but the absence of variable atmospheric thermal forcing offers a unique opportunity to infer where subsurface thermocline variability might have an effect on the SST because most of the SST variance in the model can be attributed to subsurface effects where Ekman transport plays a secondary role. A major SST anomaly center exists on the Kuroshio and its extension in the northwestern North Pacific subtropical gyre, coinciding with the subsurface variance maximum (Fig. 17). The baroclinic Rossby waves excited by Ekman pumping to the east is the cause of the westward intensified subsurface anomaly center, as suggested by Miller et al. (1998) and Deser et al. (1999). In the 10°–20°N latitude band, by contrast, we see a meridional minimum in SST rms variance despite maximum variance at 200 m. The decoupling of SST and subsurface variations results from the prevailing Ekman downwelling that shuts off the thermocline effect on SST. In such Ekman downwelling regions, surface heat flux variability is likely to dominate as a major mechanism of SST variability (Xie et al. 1999). This is in sharp contrast to the equatorial region where the upwelling effectively communicates thermocline variability by oceanic waves to the sea surface as in the ENSO (e.g., Xie et al. 1989; see Neelin et al. 1998 for a later review).

In the northwestern North Pacific, intense winter cooling allows a seasonal communication between the subsurface and surface. This window of communication closes and SST variance approaches zero in other seasons (dashed line in the right panel). Preliminary heat budget analysis indicates that advection by geostrophic currents is responsible for most mixed layer temperature anomalies. This dynamic mechanism for SST change supports the notion that SST variability observed on the Pacific Subarctic Front is statistically independent of that in the subtropics (Nakamura et al. 1997). Surface Ekman transport plays a secondary role in the decadal SST variability over the Kuroshio Extension/Subarctic Front, but its effect increases on shorter timescales, particularly over the central North Pacific.

A key issue in coupled modeling of North Pacific decadal/interdecadal variability is what is the ocean memory and where it is accessed by the atmosphere. Over much of the North Pacific subtropical gyre, the general Ekman downwelling keeps subsurface variability from interacting with the atmosphere. Our results suggest that the northwestern (Kuroshio and its extension) subtropical gyre may be a key region where subsurface variability can impact SST. If the memory of extratropical variability gives rise to the decadal/interdecadal timescales, this memory is likely to be retrieved in the equatorial Pacific and/or in the Kuroshio and its extension. The former implicates a subtropical–tropical water pathway as the oceanic memory (McCreary and Lu 1994; Liu et al. 1994), while the latter calls for midlatitude Rossby waves. It is conceivable that the Gulf Stream and North Atlantic Current also offer such a seasonal window of ocean–atmosphere coupling, which can be tested with a similar GCM run in the Atlantic basin.

Surface heat flux is a major mechanism for SST variability over much of the North Pacific subtropical gyre. Introducing atmospheric thermal forcing will almost certainly affect the subsurface variability in the central subtropical gyre as thermally forced temperature anomalies are advected along the same route as the central mode waters (Nonaka et al. 2000; Schneider et al. 1999a,b). We intend to investigate these effects of surface thermal forcing in the near future.

Acknowledgments. The four of us dedicate this paper to T.K. who left us too young and too early to see the fruits of his tireless efforts. We thank Jay McCreary, Bo Qiu, Fei-Fei Jin, Tomowo Watanabe, and Zhengyu Liu for helpful discussions; Fred Bingham, Art Miller, and an anonymous referee for comments that led to improved presentation; H. Noguchi and H. Sumata for

assistance in setting up the model. Supported by grants from the Japanese Ministry of Education, University of Tokyo's Center for Climate System Research, and Frontier Research System for Global Change that is funded by Japan Science and Technology Agency.

REFERENCES

Anderson, D. L. T., and A. E. Gill, 1975: Spin-up of a stratified ocean, with application to upwelling. *Deep-Sea Res.,* **22,** 583–596.

Bingham, F. M., 1992: The formation and spreading of subtropical mode water in the North Pacific. *J. Geophys. Res.,* **97,** 11 177–11 189.

Cox, M. D., 1987: Isopycnal diffusion in a *z*-coordinate ocean model. *Ocean Modelling* (unpublished manuscripts), **74,** 1–5.

Deser, C., M. A. Alexander, and M. S. Timlin, 1996: Upper-ocean thermal variations in the North Pacific during 1970–1991. *J. Climate,* **9,** 1840–1855.

——, ——, and ——, 1999: Evidence for a wind-driven intensification of the Kuroshio Current Extension from the 1970s to the 1980s. *J. Climate,* **12,** 1697–1706.

Graham, N. E., 1994: Decadal scale variability in the 1970s and 1980s: Observations and model results. *Climate Dyn.,* **10,** 135–162.

Gu, D., and S. G. H. Philander, 1997: Internal climate fluctuations that depend on exchanges between the tropics and extratropics. *Science,* **275,** 805–807.

Hautala, S. L., and D. H. Roemmich, 1998: Subtropical mode water in the Northeast Pacific basin. *J. Geophys. Res.,* **103,** 13 055–13 066.

Huang, R. X., and B. Qiu, 1994: Three-dimensional structure of the wind-driven circulation in the subtropical North Pacific. *J. Phys. Oceanogr.,* **24,** 1608–1622.

——, and J. Pedlosky, 1999: Climate variability inferred from a layered model of the ventilated thermocline. *J. Phys. Oceanogr.,* **29,** 779–790.

Inui, T., K. Takeuchi, and K. Hanawa, 1999: A numerical investigation of the subduction process in response to an abrupt intensification of westerlies. *J. Phys. Oceanogr.,* **29,** 1993–2015.

Jin, F.-F., 1997: A theory of interdecadal climate variability of the North Pacific ocean–atmosphere system. *J. Climate,* **10,** 1821–1835.

Kalnay, E., and Coauthors, 1996: The NCEP/NCAR 40-Year Reanalysis Project. *Bull. Amer. Meteor. Soc.,* **77,** 437–471.

Kleeman, R., J. P. McCreary, and B. A. Klinger, 1999: A mechanism for generating ENSO decadal variability. *Geophys. Res. Lett.,* **26,** 1743–1746.

Knutson, T. R., and S. Manabe, 1998: Model assessment of decadal variability and trends in the tropical Pacific Ocean. *J. Climate,* **11,** 2273–2296.

Kubokawa, A., 1999: Ventilated thermocline strongly affected by a deep mixed layer: A theory for subtropical countercurrent. *J. Phys. Oceanogr.,* **29,** 1314–1333.

——, and T. Inui, 1999: Subtropical countercurrent in an idealized ocean GCM. *J. Phys. Oceanogr.,* **29,** 1303–1313.

Latif, M., and T. P. Barnett, 1994: Causes of decadal climate variability over the North Pacific and North America. *Science,* **266,** 634–637.

Levitus, S., 1982: *Climatological Atlas of the World Ocean.* NOAA Prof. Paper No. 13, U.S. Govt. Printing Office, 173 pp.

Liu, Z., 1993: Thermocline forced by varying Ekman pumping. Part II: Annual and decadal Ekman pumping. *J. Phys. Oceanogr.,* **23,** 2523–2540.

——, 1999: Forced planetary wave response in a thermocline gyre. *J. Phys. Oceanogr.,* **29,** 1036–1055.

——, S. G. H. Philander, and R. C. Pacanowski, 1994: A GCM study of the tropical–subtropical upper-ocean water exchange. *J. Phys. Oceanogr.,* **24,** 2606–2623.

Luyten, J. R., J. Pedlosky, and H. Stommel, 1983: The ventilated thermocline. *J. Phys. Oceanogr.,* **13,** 292–309.

Mantua, N. J., S. R. Hare, Y. Zhang, J. M. Wallace, and R. C. Francis, 1997: A Pacific interdecadal climate oscillation with impacts on salmon production. *Bull. Amer. Meteor. Soc.,* **78,** 1069–1079.

Marshall, J. C., and A. J. G. Nurser, 1991: A continuously stratified thermocline model incorporating a mixed layer of variable depth and density. *J. Phys. Oceanogr.,* **21,** 1780–1792.

McCartney, M. S., 1982: The subtropical recirculation of mode waters. *J. Mar. Res.,* **40,** 427–464.

McCreary, J. M., and P. Lu, 1994: Interaction between the subtropical and equatorial ocean circulations: The subtropical cell. *J. Phys. Oceanogr.,* **24,** 466–497.

Miller, A. J., D. R. Cayan, T. P. Barnett, N. E. Graham, and J. M. Oberhuber, 1994: Interdecadal variability of the Pacific Ocean: Model response to observed heat flux and wind stress anomalies. *Climate Dyn.,* **9,** 287–302.

——, ——, and W. B. White, 1998: A westward-intensified decadal change in the North Pacific thermocline and gyre-scale circulation. *J. Climate,* **11,** 3112–3127.

Minobe, S., 1997: A 50–70-year climatic oscillation over the North Pacific and North America. *Geophys. Res. Lett.,* **24,** 683–686.

Nakamura, H., G. Lin, and T. Yamagata, 1997: Decadal climate variability in the North Pacific during recent decades. *Bull. Amer. Meteor. Soc.,* **78,** 2215–2225.

Nakamura, H.-H., 1996: A pycnostad on the bottom of the ventilated portion in the central subtropical North Pacific: Its distribution and formation. *J. Oceanogr.,* **52,** 171–188.

Neelin, J. D., and W. Weng, 1999: Analytical prototypes for ocean–atmosphere interaction at midlatitudes. Part I: Coupled feedbacks as a sea surface temperature dependent stochastic process. *J. Climate,* **12,** 697–721.

——, D. S. Battisti, A. C. Hirst, F.-F. Jin, Y. Wakata, T. Yamagata, and S. E. Zebiak, 1998: ENSO theory. *J. Geophys. Res.,* **103,** 14 261–14 290.

Nitta, T., and S. Yamada, 1989: Recent warming of tropical sea surface temperature and its relationship to the Northern Hemisphere circulation. *J. Meteor. Soc. Japan,* **67,** 375–382.

Nonaka, M., S.-P. Xie, and K. Takeuchi, 2000: Equatorward spreading of a passive tracer with application to North Pacific interdecadal temperature variations. *J. Oceanogr.,* **56,** 173–183.

Pacanowski, R. C., K. W. Dixon, and A. Rosati, 1991: The GFDL Modular Ocean Model user guide. GFDL Ocean Group Tech. Rep. 2. [Available from GFDL, P.O. Box 308, Princeton, NJ 08542-0308.]

Polovina, J. J., G. T. Mitchum, and G. T. Evans, 1995: Decadal and basin-scale variation in mixed layer depth and the impact on biological production in the central and North Pacific, 1960–1988. *Deep-Sea Res.,* **42,** 1701–1716.

Qiu, B., 2000: Interannual variability of the Kuroshio extension system and its impact on the wintertime SST field. *J. Phys. Oceanogr.,* **30,** 1486–1502.

——, and R. X. Huang, 1995: Ventilation of the North Atlantic and North Pacific: Subduction versus obduction. *J. Phys. Oceanogr.,* **25,** 2374–2390.

Robertson, A. W., 1996: Interdecadal variability over the North Pacific in a multi-century climate simulation. *Climate Dyn.,* **12,** 227–241.

Schneider, N. S., A. J. Miller, M. A. Alexander, and C. Deser, 1999a: Subduction of decadal North Pacific temperature anomalies: Observations and dynamics. *J. Phys. Oceanogr.,* **29,** 1056–1070.

——, S. Venzke, A. J. Miller, D. W. Pierce, T. P. Barnett, C. Deser, and M. Latif, 1999b: Pacific thermocline bridge revisited. *Geophys. Res. Lett.,* **26,** 1329–1332.

Shuto, K., 1996: Interannual variations of water temperature and salinity along the 137°E meridian. *J. Oceanogr.,* **52,** 575–596.

Suga, T., and K. Hanawa, 1990: The mixed-layer climatology in the northwestern part of the North Pacific subtropical gyre and the formation area of subtropical mode water. *J. Mar. Res.,* **48,** 543–566.

——, Y. Takei, and K. Hanawa, 1997: Thermostad distribution in the North Pacific subtropical gyre: The central mode water and the subtropical mode water. *J. Phys. Oceanogr.,* **27,** 140–152.

Talley, L. D., 1988: Potential vorticity distribution in the North Pacific. *J. Phys. Oceanogr.,* **18,** 89–106.

Tanimoto, Y., N. Iwasaka, K. Hanawa, and Y. Toba, 1993: Characteristic variations of sea surface temperature with multiple time scales in the North Pacific. *J. Climate,* **6,** 1153–1160.

——, ——, and ——, 1997: Relationships between sea surface temperature, the atmospheric circulation and air–sea fluxes on multiple time scales. *J. Meteor. Soc. Japan,* **75,** 831–849.

Trenberth, K. E., and J. W. Hurrel, 1994: Decadal atmosphere–ocean variations in the Pacific. *Climate Dyn.,* **9,** 303–319.

White, W. B., 1995: Design of a global observing system for gyre-scale upper ocean temperature variability. *Progress in Oceanography,* Vol. 36. Pergamon, 169–217.

Williams, R. G., 1991: The role of the mixed layer in setting the potential vorticity of the main thermocline. *J. Phys. Oceanogr.,* **21,** 1803–1814.

Xie, S.-P., 1995: Interaction between the annual and interannual variations in the equatorial Pacific. *J. Phys. Oceanogr.,* **25,** 1930–1941.

——, A. Kubokawa, and K. Hanawa, 1989: Oscillations with two feedback processes in a coupled ocean–atmosphere model. *J. Climate,* **2,** 946–964.

——, Y. Tanimoto, H. Noguchi, and T. Matsuno, 1999: How and why climate variability differs between the tropical Atlantic and Pacific. *Geophys. Res. Lett.,* **26,** 1609–1612.

Yasuda, T., and K. Hanawa, 1997: Decadal changes in the mode waters in the midlatitude North Pacific. *J. Phys. Oceanogr.,* **27,** 858–870.

Yukimoto, S., M. Endoh, Y. Kitamura, A. Kitoh, T. Motoi, A. Noda, and T. Tokioka, 1996: Interannual and interdecadal variabilities in the Pacific in a MRI coupled GCM. *Climate Dyn.,* **12,** 667–683.

Zhang, R.-H., and S. Levitus, 1997: Structure and cycle of decadal variability of upper-ocean temperature in the North Pacific. *J. Climate,* **10,** 710–727.